Pramāṇa, Vol. 24, No. 6, June 1985, pp. 875–886. © Printed in India.

Focussing and defocussing of ballistic phonons in diamond and Nb_3Sn

A PUSHPAHASAN and K S VISWANATHAN
Department of Physics, University of Kerala, Kariavattom, Trivandrum 695 581, India

MS received 16 November 1984

Abstract. The ballistic propagation of phonons in diamond and Nb_3Sn at 40 and at 4·2 K is examined. The nature of variation of the phonon magnification factor has been analysed both in the wave vector as well as group velocity spaces. Using the Polar Schmidt-net with Pole at $(\pi/2, \pi/2)$, the mappings of phonon focussing and defocussing are made. It is shown that the mapping for the FTA mode for Nb_3Sn exhibits islands acting as impenetrable barriers for phonon propagation.

Keywords. Acoustic phonons; focussing; defocussing; mapping of phonons; polar Schmidt-net; impenetrable regions.

PACS No. 63·20

1. Introduction

The ballistic propagation of phonons in crystals at very low temperatures has been verified during the last two decades in a variety of experiments. If a crystal is cooled below its superconducting critical temperature, thermal transport is dominated by phonon scattering processes. Further, if the crystal is free from defects, impurity scattering is reduced to the minimum. Under these circumstances the phonon mean free path is limited only by the linear dimensions of the crystal and phonons propagate ballistically.

In their heat pulse experiments, Taylor *et al* (1969, 1971) reported very large differences in the intensity of phonons of different polarizations propagating ballistically in elastically anisotropic crystals such as LiF, KCl and Al_2O_3. Their experiments showed that the energy flow was enhanced along certain directions even though the original angular distribution of the wave vectors was isotropic. The recent surge of interest in phonon imaging (Hensel and Dynes 1979; Northrop and Wolfe 1979, 1980; Einsenmenger 1980, 1981; Wolfe *et al* 1980; Eichele *et al* 1982a, b; Every *et al* 1984)—a technique that employs ballistic phonons to probe the effects of elastic anisotropy and surface scattering on phonon transport—has brought out the remarkable directional anisotropy of ballistic phonons and the phonon wind in elastically anisotropic solids. Measurements of the thermal conductivity of Si and CaF_2 in the boundary-scattering regime demonstrated anisotropies of up to 50% for Si and 40% for CaF_2 (McCurdy *et al* 1970). Striking differences in the boundary-scattered phonon conductivity and effective phonon mean free path were predicted along the principal axes of cubic crystals (McCurdy 1982). A behaviour no less complex is to be expected in many, if not most, crystals.

The above interesting results arise from phonon focussing. In elastically anisotropic

substances, barring a few symmetry directions, the ray velocity or the group velocity of the acoustic waves is not parallel to the phase velocity. The angular deviation between the ray velocity direction and phase velocity direction depends upon the direction of the wave vector, **q**, the phonon polarization and the elastic anisotropy. Phonon focussing occurs when the direction of the group velocity varies more slowly over some small solid angle with wave vector direction than for an elastically isotropic solid. Since the energy flow is in the direction of the ray (group) velocity vector, the phonon flux is enhanced along any strongly focussed directions.

The focussing of phonons in crystals has been studied by several authors in recent years (Maris 1971; Philip and Viswanathan 1978; Every 1980; Northrop and Wolfe 1980).

According to Maris (1971) the phonon magnification factor (PMF), A, for a particular polarization is defined as

$$A = \mathrm{d}\Omega_q/\mathrm{d}\Omega_s, \tag{1}$$

where $\mathrm{d}\Omega_q$ is the solid angle in the wave vector space and $\mathrm{d}\Omega_s$ is the corresponding solid angle in the group velocity space. Philip and Viswanathan (1978) showed that

$$A^{-1} = J\,(\sin\theta_s/\sin\theta), \tag{2}$$

where

$$J = \left(\frac{\mathrm{d}\theta_s\,\mathrm{d}\phi_s}{\mathrm{d}\theta\,\mathrm{d}\phi}\right) = \frac{\partial\theta_s}{\partial\theta}\frac{\partial\phi_s}{\partial\phi} - \frac{\partial\theta_s}{\partial\phi}\frac{\partial\phi_s}{\partial\theta} \tag{3}$$

is none other than the Jacobian of the transformation relating the polar variables (θ_s, ϕ_s) of the group velocity vector and (θ, ϕ) of the wave vector.

The direction of the energy flow (θ_s, ϕ_s) depends on the group velocity components which again depend on (θ, ϕ). So θ_s and ϕ_s are functions of θ and ϕ. Hence analytical expressions in terms of θ and ϕ can be derived for J and therefore for A also. Further, the Gaussian curvature K of the slowness surface can be expressed in terms of the inverse PMF, the wave vector and the angular deviation between the ray vector and the wave vector (Lax and Narayanamurti 1980). Thus for any given set of values of θ and ϕ, A and K can be evaluated numerically. But, often, the experimental results relate to the phonon focussing in the group velocity space. To enable comparison of the theoretically calculated values of phonon focussing with the experimental results, it is necessary to evaluate $A\,(\theta_s, \phi_s)$ rather than $A\,(\theta, \phi)$. However, it is not possible to obtain analytical expressions for the PMF as a function of the variables θ_s and ϕ_s. Nevertheless, $A\,(\theta_s, \phi_s)$ can be evaluated numerically by first evaluating $A\,(\theta, \phi)$ for a given set of values of θ and ϕ and thereafter by sorting the computer output for $A\,(\theta, \phi)$ in ascending value for either of the parameters θ_s or ϕ_s. This is the procedure for numerical evaluation adopted in the present paper in which we give the results of the numerical calculations for diamond and for non-transforming Nb_3Sn.

2. Numerical procedure

A computer program was written to evaluate the magnitudes of the group and the inverse phase velocities, the polar variables θ_s and ϕ_s of the group velocity vector, the

angular deviation Δ between the ray vector direction and the wave vector direction, the Gaussian curvature K of the slowness surface and the magnification factor A, for propagation along any general direction (θ, ϕ) inside the crystal. The computer was instructed to calculate and print all the above nine parameters in intervals of 5° for both θ and ϕ.

As stated earlier the magnification factor A (θ_s, ϕ_s) evaluated as a function of the group velocity variables is more useful for comparison with the available experimental data rather than A (θ, ϕ). While the values of θ and ϕ are varied uniformly and in intervals of 5°, the corresponding directions θ_s and ϕ_s are decided by the anisotropic elastic properties of the crystal. Hence θ_s and ϕ_s do not have a uniform distribution in group velocity space. Thus we have a non-uniform set of values for the group velocity variables θ_s and ϕ_s which are densely populated in certain regions and sparsely distributed in other regions.

The data for A (θ, ϕ) in increasing order for the variables θ and ϕ was stored in magnetic tapes. Thereafter data for A (θ_s, ϕ_s), in ascending order for either the variables θ_s or ϕ_s, was also obtained and stored in magnetic tapes by sorting the former data in magnetic tapes using the built-in Subroutine of a TDC-316 computer. Thus the sorted output gives the magnification factor A (θ_s, ϕ_s) for different directions in the group velocity space. This output can be compared directly with the figures obtained by the ballistic phonon imaging techniques or other similar methods.

As $\sin\theta$ and $\sin\theta_s$ are positive throughout, the magnification factor $A[=(J)^{-1}(\sin\theta/\sin\theta_s)]$ takes the sign of the Jacobian J. But only the magnitude of A (*i.e.* $|A|$) has physical significance and hence only that is shown in our diagrams. Curves showing the relation between $|A|$ and θ_s, ϕ_s, θ or ϕ are drawn only in the range 0° to 90° for the angular variables in view of the cubic symmetry.

3. Phonon focussing in diamond

Though diamond has been extensively studied and is regarded as the test ground for various theories, it still offers scope for further work. The ballistic propagation of phonons in diamond is but one example. For our numerical calculations we used the following values of the elastic stiffness constants as given by Auld (1973). They are $c_{11} = 102 \times 10^{10}\ \mathrm{Nm}^{-2}$, $c_{12} = 25 \times 10^{10}\ \mathrm{Nm}^{-2}$ and $c_{44} = 49{\cdot}2 \times 10^{10}\ \mathrm{Nm}^{-2}$.

The computer output shows that diamond does not exhibit any unusual focussing properties. The PMF is never too large for any direction inside the crystal as compared to other crystals such as Nb_3Sn, Ge, etc. The longitudinal acoustic (LA) mode is nearly "isotropic" showing neither very high nor very small values for the PMF. Even the slow transverse acoustic (STA) and fast transverse acoustic (FTA) modes do not show very large or very low values for the PMF.

The PMF for the LA mode is positive throughout. In figure 1 we show in four curves the relation between $|A|$ and θ_s or θ in some of the principal meridian planes for the LA mode. Each of the four curves is symmetric about the [010] direction. Further, the computer output shows that the phonon focussing for the LA mode is nearly "isotropic" with values of A lying in the range 0·40 to 1·65. The minimum (0·40) is along the [001] and [001] directions and the maximum value (1·65) is along the $\langle 111 \rangle$ directions—a fact which is evident from figure 1 also.

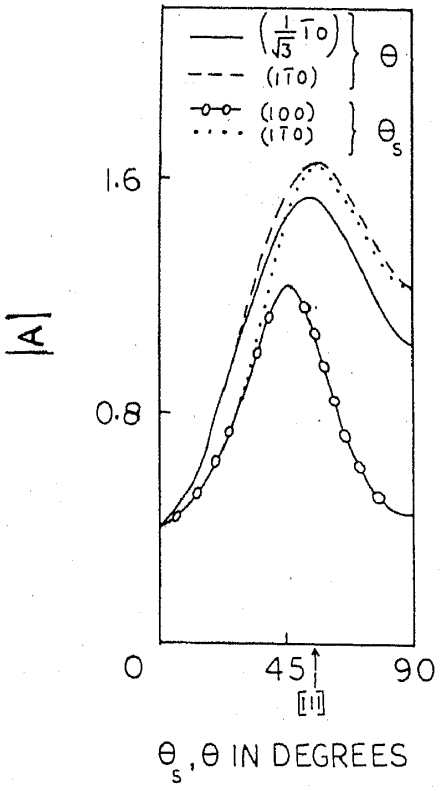

Figure 1. Relation between $|A|$ and θ_s or θ in some of the principal meridian planes for the LA mode in diamond.

Of the three phonon acoustic modes in a crystal, the ray velocity and slowness surfaces for the STA mode have the most interesting topological properties. Also the PMF for this mode exhibits interesting variations. As mentioned earlier, we have to rearrange the data for $A(\theta, \phi)$ in order to obtain $A(\theta_s, \phi_s)$. It is not possible to show the variation of $|A|$ against any precise value of the variables θ_s or ϕ_s except along the symmetry planes. However, experiments on phonon focussing measure the intensity of the phonon flux over a small solid angle in the group velocity space. So in figure 2 we show the relation between $|A|$ and ϕ_s over a small range of 3·3° for the variable θ_s (*i.e.*, $2{\cdot}3° \leqslant \theta_s \leqslant 5{\cdot}6°$). In other words, we show the propagation of the phonon flux within a conical region defined by $2{\cdot}3° \leqslant \theta_s \leqslant 5{\cdot}6°$. It is seen that the PMF has sharp peaks having the maximum value of 30 along $\phi_s = 11{\cdot}3°, 78{\cdot}7°, \ldots$, and other symmetric directions. Further, the PMF also shows a secondary maxima (21·5) along $\phi_s = 27{\cdot}3°, 62{\cdot}7°$, etc. It is thus evident that even within this small conical region, the ballistic phonons are focussed only along specific directions. The STA mode for non-transforming Nb_3Sn at 4·2 K (figure 9) also has a similar behaviour.

For propagation in a principal symmetry plane, the group velocity vector also lies in the same plane. Figure 3 shows the relation between $|A|$ and ϕ_s in the (001) plane for the FTA mode. The PMF does not show very high values for this mode as in the STA mode. The maximum value (4·5) of the PMF is along the $\langle 100 \rangle$ directions. The minimum value (1·96) is along the directions $\phi_s = 7{\cdot}1°, 82{\cdot}9°$, etc. Along all other directions in this plane the PMF keeps an almost constant value of 3·2.

Our computer output shows that the PMF for diamond has a maximum value of 57 which is reached for the STA mode for propagation along regions having $\theta = 75°$ or

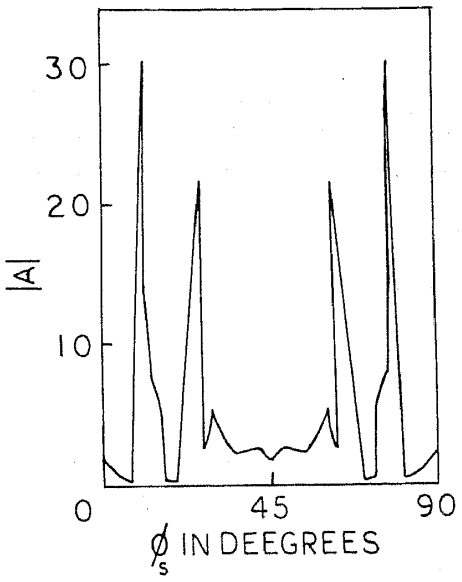

Figure 2. Relation between $|A|$ and ϕ_s in the conical region defined by $2{\cdot}3° \leqslant \theta_s \leqslant 5{\cdot}6°$ for the STA mode in diamond.

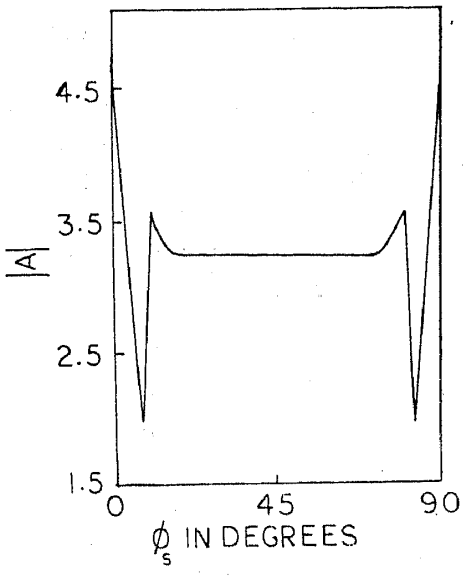

Figure 3. Relation between $|A|$ and ϕ_s in the (001) plane for the FTA mode in diamond.

115°. So in figure 4 we show the relation between $|A|$ and ϕ at $\theta = 75°$ for the three acoustic modes of diamond. It is obvious that the maximum value of the PMF is for the STA mode and that too along $\phi = 10°, 80°$, etc. while along $\phi = 45°, 135°$, etc. the PMF has the minimum value (0·45). The curve for the STA mode is similar to that shown in figure 2 wherein we have shown the relation between $|A|$ and ϕ_s in a small range of values for θ_s. For the FTA mode the PMF has a maximum (3·25) along $\phi = 0°, 90°$, etc.—the directions along which the STA mode has a local minimum. As is to be expected, the PMF for the LA mode is small, nearly "isotropic", but is oscillatory. All the three curves are symmetric about the directions $\phi = 45°, 90°$, etc.

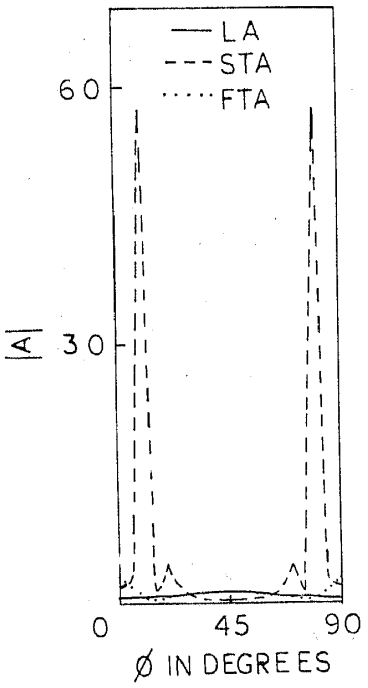

Figure 4. Relation between $|A|$ and ϕ at $\theta = 75°$ for the three acoustic modes of diamond.

4. Phonon focussing in non-transforming Nb_3Sn

The A-15 compounds have very interesting elastic properties. These compounds are characterized by high superconducting critical temperatures. In these compounds the STA mode propagating along the face diagonal or the [110] direction with $[1\bar{1}0]$ polarization becomes soft at low temperatures. Sections of the ray velocity and slowness surfaces in the (001) and (110) planes of A-15 compounds have earlier been studied by Philip and Viswanathan (1977). They have reported that the A-15 compounds exhibit unusually large cuspidal edges for the ray velocity surfaces at temperatures below superconducting critical temperatures. In this section we report the results of our study of the phonon magnification for a typical A-15 compound, namely, non-transforming Nb_3Sn at two different temperatures—at 40 K, and also at 4·2 K where the relation $c_{11} = c_{12}$ strictly holds good. For our numerical calculations we adopted the following values of the elastic stiffness constants as given by Testardi (1973). They are $c_{11} = 17{\cdot}18 \times 10^{10}\,\mathrm{Nm}^{-2}$, $c_{12} = 16{\cdot}11 \times 10^{10}\,\mathrm{Nm}^{-2}$ and $c_{44} = 2{\cdot}717 \times 10^{10}\,\mathrm{Nm}^{-2}$ at 40 K and $c_{11} = c_{12} = 16{\cdot}46 \times 10^{10}\,\mathrm{Nm}^{-2}$ and $c_{44} = 2{\cdot}66 \times 10^{10}\,\mathrm{Nm}^{-2}$ at 4·2 K.

In figure 5 we show the relation between $|A|$ and ϕ_s in the (001) plane for the STA mode at 40 K. The PMF has a maximum value of 50 along $\phi_s = 22{\cdot}6°, 67{\cdot}4°$, etc. An interesting feature is that the magnification is almost zero (0·02) in regions defined by $32° \leqslant \phi_s \leqslant 58°$ and other equivalent symmetry regions.

In figure 6 we show the relation between $|A|$ and ϕ_s in the (001) plane for the STA mode at 4·2 K. We find that the PMF has been reduced and the directions of maxima have also

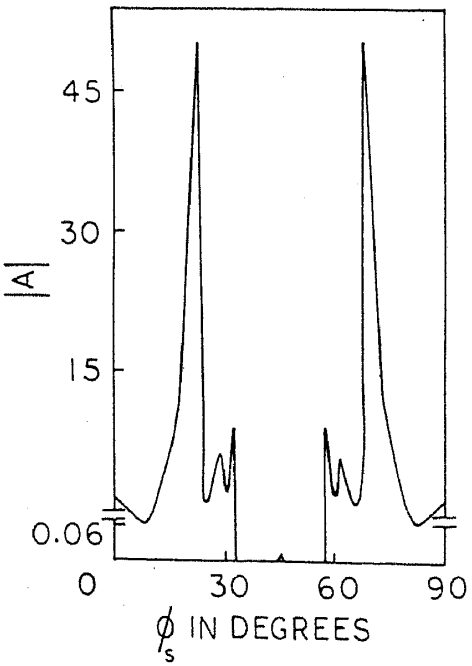

Figure 5. Relation between $|A|$ and ϕ_s in the (001) plane for the STA mode in non-transforming Nb_3Sn at 40 K. The curve in the range $0 \leqslant |A| \leqslant 0{\cdot}06$ is drawn in a magnified scale for showing the finer details of the phonon focussing and defocussing aspects about the [110] direction.

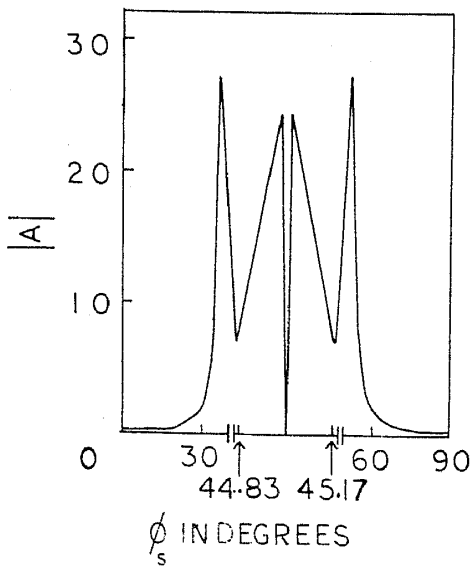

Figure 6. Relation between $|A|$ and ϕ_s in the (001) plane for the STA mode in non-transforming Nb_3Sn at 4·2 K. For showing the strong defocussing along the [110] direction where the mode becomes soft and the accompanying strong focussing about both sides of the [110] direction, the curve in the range $44{\cdot}83° \leqslant \phi_s \leqslant 45{\cdot}17°$ is drawn in a magnified scale.

been altered. A striking feature is that the PMF is zero along the $\langle 110 \rangle$ directions wherein this mode becomes soft. In contrast to the behaviour of the STA phonons at 40 K, the STA phonons are focussed strongly along $\phi_s = 44{\cdot}98°, 45{\cdot}02°$, etc. at 4·2 K. As before the curve is symmetric about the [110] direction.

In figure 7 we show the relation between Δ (the angular deviation of the ray vector direction vis-a-vis the wave vector direction) and ϕ in the (001) plane for the STA mode at 40 K and at 4·2 K. This angular deviation is zero for propagation along the $\langle 001 \rangle$ and $\langle 110 \rangle$ directions (pure mode directions), but, can be as high as 59·8° at 40 K and 85° at 4·2 K. These curves too are symmetric about the face diagonal.

Figure 8 shows the relation between $|A|$ and θ_s or θ in the (110) plane for the STA mode at 40 K. From the relation between $|A|$ and θ_s it is seen that the phonons are channelled mainly along $\theta_s = 0°, 18{\cdot}8°, 20{\cdot}8°$ and the corresponding symmetry directions. There are virtually no phonons propagating in the range $40° \leqslant \theta_s \leqslant 90°$ and in the corresponding symmetric range $90° \leqslant \theta_s \leqslant 140°$. Thus the variation of $|A|$ against θ_s shows sharp peaks accompanied by secondary peaks. The curve depicting $|A|$ *vs* θ has a totally different pattern showing peaks along $\theta = 0°, 20°, 60°$ and equivalent symmetric directions.

In figure 9 we show the relation between $|A|$ and ϕ_s in the narrow conical region defined by $43{\cdot}5° \leqslant \theta_s \leqslant 46{\cdot}5°$ for the STA mode at 4·2 K. The PMF is high only for the regions defined by $0° \leqslant \phi_s \leqslant 23{\cdot}5°$ and other equivalent regions. In the regions $24° \leqslant \phi_s \leqslant 66°$ and other equivalent regions, the focussing is zero except along $\phi_s = 44{\cdot}3°, 45{\cdot}7°$, etc. The maximum PMF (24·2) is along $\phi_s = 0°, 90°$, etc. for this region.

Unlike the STA phonons the LA phonons do not show any tendency for sharp focussing or defocussing along any direction. Figure 10 shows the relation between $|A|$ and θ_s or θ in the $(1\bar{1}0)$ and (010) planes at 40 K and also at 4·2 K. As in the LA phonons in diamond, A for the LA phonons in non-transforming Nb_3Sn is positive throughout, for propagation at both the temperatures considered. The PMF varies continuously from 0·32 to 1·86 at 40 K and from 0·28 to 2·17 at 4·2 K. Just as for diamond the maxima are along the $\langle 111 \rangle$ directions and the minima are along the [001] and $[00\bar{1}]$ directions.

In figure 11 we show the relation between $|A|$ and ϕ_s in the (001) plane for the FTA mode both at 40 K and at 4·2 K. Except along the $\langle 100 \rangle$ directions where peaks (1·4 at 40 K and 0·52 at 4·2 K) are obtained, the PMF keeps an almost uniform value (0·66 at 40 K and 0·46 at 4·2 K) throughout for propagation in the (001) plane. The curves are also symmetric about the face diagonal.

Nevertheless, the FTA mode at 4·2 K shows high and sharp focussing along certain regions. An example of that feature is shown in figure 12 where $|A|$ is plotted against ϕ_s in the conical region defined by $66{\cdot}79° \leqslant \theta_s \leqslant 67{\cdot}94°$. Similar to the behaviour of the STA mode at 4·2 K (figure 9) the FTA mode at 4·2 K also shows sharp focussing only along specific directions, namely, $\phi_s = 22{\cdot}89°, 67{\cdot}11°$, etc.

5. Mapping of phonon focussing and defocussing

The PMF shows very high values for certain directions and similarly is almost zero in certain other regions. The phenomenon of focussing itself depends on two factors. First, the distribution of the polar variables of the group velocity vector (θ_s, ϕ_s) may be densely populated around certains directions. Secondly, the PMF exhibits unusually high values of the order of 10^3 or 10^4 for some directions. These are to be attributed to

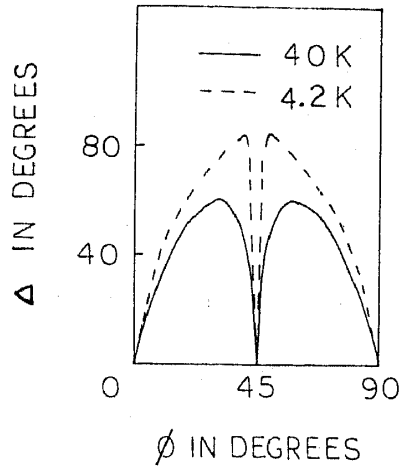

Figure 7. Relation between Δ (the angular deviation of the ray vector direction vis-a-vis the wave vector direction) and ϕ in the (001) plane for the STA mode in non-transforming Nb_3Sn.

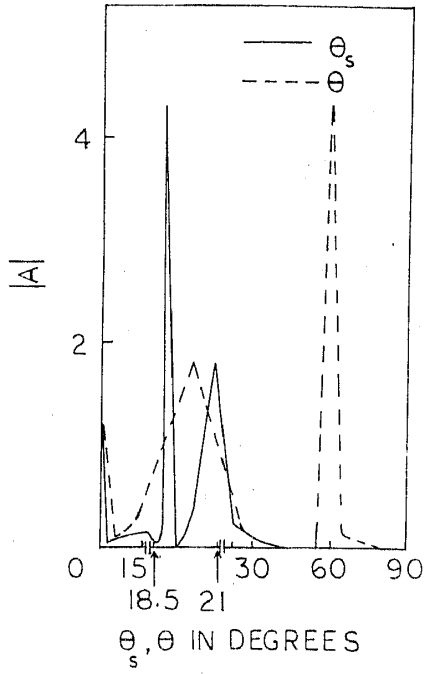

Figure 8. Relation between $|A|$ and θ_s or θ in the (110) plane for the STA mode in non-transforming Nb_3Sn at 40 K. For showing the defocussing aspects with greater clarity the curves in the range $18{\cdot}5° \leqslant \theta_s$ (or θ) $\leqslant 21°$ are drawn in a magnified scale.

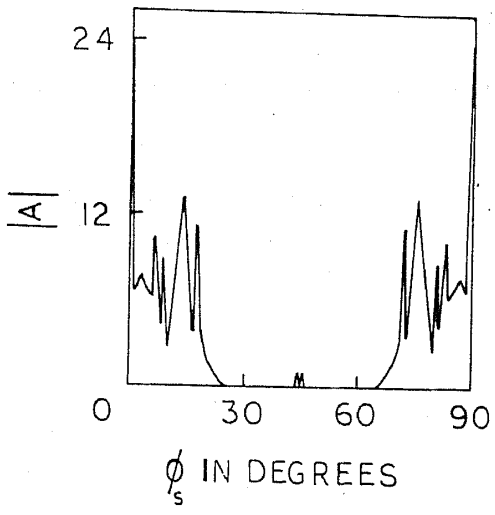

Figure 9. Relation between $|A|$ and ϕ_s in the conical region defined by $43{\cdot}5° \leqslant \theta_s \leqslant 46{\cdot}5°$ for the STA mode in non-transforming Nb_3Sn at 4·2 K.

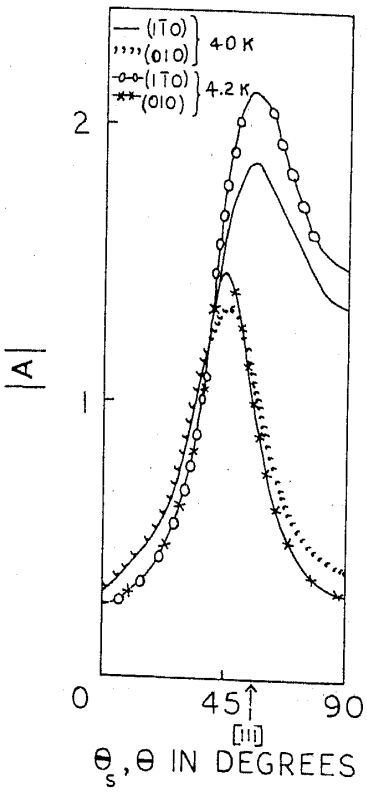

Figure 10. Relation between $|A|$ and θ_s or θ in the $(1\bar{1}0)$ and (010) planes for the LA mode in non-transforming Nb_3Sn.

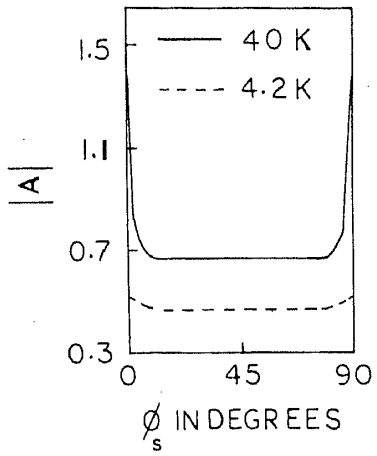

Figure 11. Relation between $|A|$ and ϕ_s in the (001) plane for the FTA mode in non-transforming Nb_3Sn.

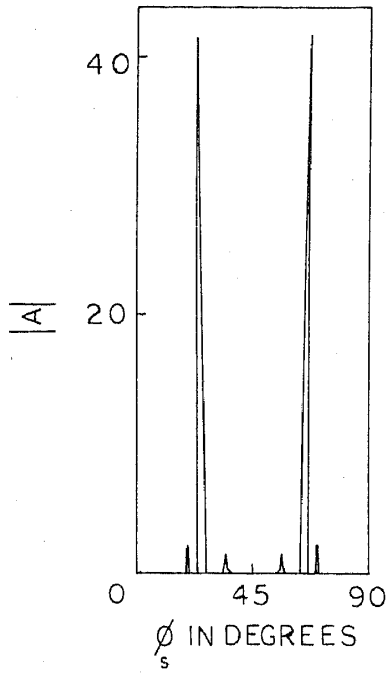

Figure 12. Relation between $|A|$ and ϕ_s in the conical region defined by $66{\cdot}79° \leqslant \theta_s \leqslant 67{\cdot}94°$ for the FTA mode in non-transforming Nb_3Sn at 4·2 K.

the shape of the ray velocity surface or the curvature of the slowness surface. The curvature tends to be very small along the directions showing large values for the PMF.

The experimental results on phonon imaging can be best understood if we plot the distribution of the angles θ_s and ϕ_s relating to the group velocity vectors as in a Lambert's zenithal equal-area projection of the world in hemispheres onto a circle (Steers 1970) or as in a Polar Schmidt-net with Pole at $(\pi/2, \pi/2)$ meant for studying the distributions of directions on a unit sphere (Selby 1964; Mardia 1972). Here the Pole is both the centre of the circular Polar Schmidt-net and also the point of contact between the sphere and the plane of projection.

Our numerical calculations described in §§3 and 4 provide us with a uniform distribution of 2628 points in the wave vector space and a corresponding number of points (θ_s, ϕ_s) in the group velocity space. Polar Schmidt-nets with Pole at $(\pi/2, \pi/2)$ were then drawn for each of the three types of acoustic modes for diamond and for non-transforming Nb_3Sn at 40K and 4·2K. Thus our Polar Schmidt-nets show the distribution of points in the group velocity space falling within the range $0° \leqslant \theta_s \leqslant 180°$ and $0° \leqslant \phi_s \leqslant 180°$. Apart from showing the density distribution of points in the group velocity space, our graphs give an idea of the magnitude of A also. Directions for which $|A|$ lies between 0 and 1 are marked by a dot. The marks $\oplus, \otimes, \supset$ and $\times$ stand for directions for which $10^{-4} \leqslant |A| < 10^{-3}$, $10^{-2} \leqslant |A| < 10^{-1}$, $1 \leqslant |A| < 10$ and $10 \leqslant |A| < 10^2$ respectively. Thus the figures give an idea of both the focussing of phonons as well as the magnitude of A. All these figures show the four fold symmetry of the crystal.

In this section we show only three Polar Schmidt-nets, one for each of the three acoustic modes, due to lack of space.

Figure 13 shows the Polar Schmidt-net for the LA phonons in non-transforming Nb_3Sn at 4·2K. The figure shows an almost uniform distribution of points as is to be

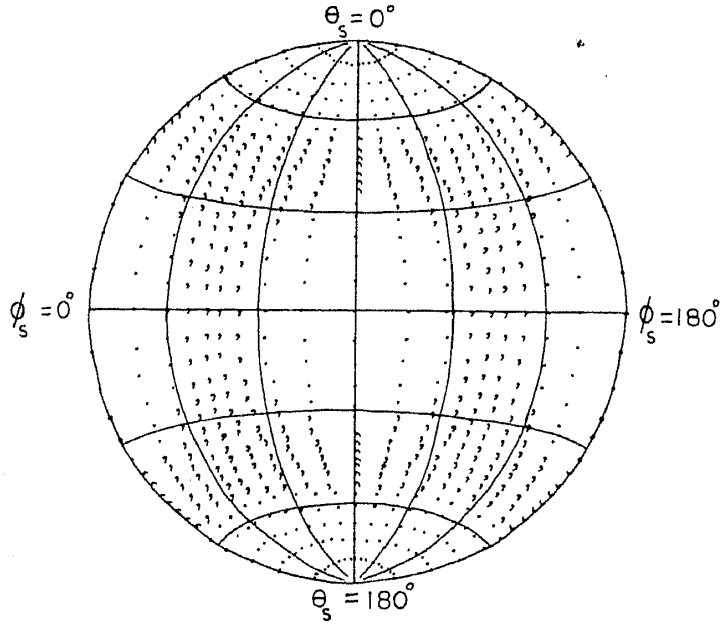

Figure 13. Polar Schmidt-net with Pole at $(\pi/2, \pi/2)$ for the LA phonons in non-transforming Nb_3Sn at 4·2 K. An explanation of the different types of markings shown in this and the two succeeding figures are given in § 5. Further, in all the three figures, the grid lines of the net are drawn at intervals of 30° for both the variables θ_s and ϕ_s.

expected for the LA modes. An interesting feature revealed for the first time is that in real space the LA phonons are focussed more or less in the regions defined by

(i) $[m\cdot 90° + 30°] \leqslant \theta_s \leqslant [(m+1)\cdot 90° - 30°]$; ϕ_s taking any value

and

(ii) $60° \leqslant \theta_s \leqslant 120°$; $(n\cdot 90° + 30°) \leqslant \phi_s \leqslant (n\cdot 90° + 60°)$

where $m = 0$ and 1 and $n = 0$, 1, 2 and 3.

In figure 14 the Polar Schmidt-net for the STA mode of diamond is shown. It shows that the density is non-uniformly distributed in space, being high along the diagonal directions and the edges of the squares and low elsewhere. However, the intensity of focussing is, relatively higher about the [001] and [00$\bar{1}$] directions.

Figure 15 is the Polar Schmidt-net for the FTA mode in non-transforming Nb_3Sn at 40 K. This figure is most interesting, not so much for the distribution of points, but for the complete absence of points in certain regions. The plot shows regions or "islands" that are empty, that is, without any group velocity vectors. This defocussing is, in fact, as much important a phenomenon as the focussing itself. This figure shows for the first time that there exist "islands" which act as impenetrable barriers for the propagation of ballistic phonons. Such regions are more often found for the FTA mode than for the other two modes.

Acknowledgement

One of the authors (AP) is thankful to the CSIR, New Delhi, for financial assistance.

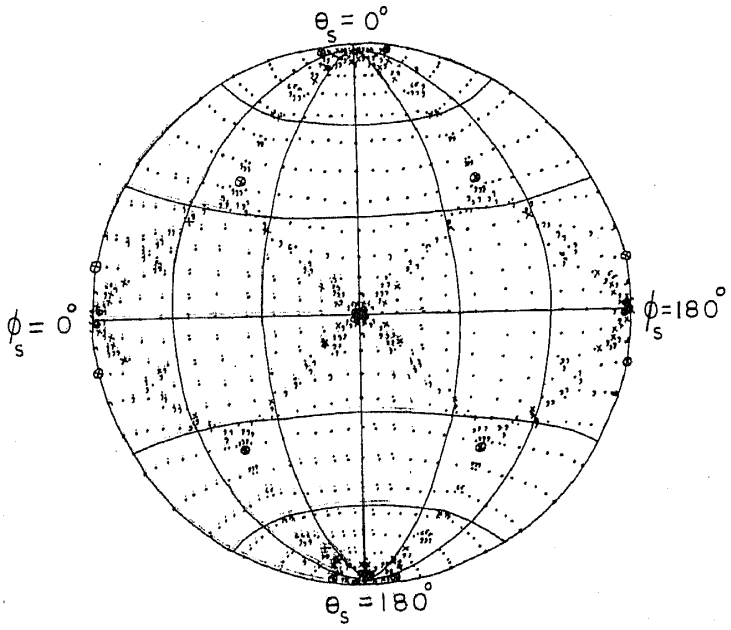

Figure 14. Polar Schmidt-net with Pole at $(\pi/2, \pi/2)$ for the STA phonons in diamond.

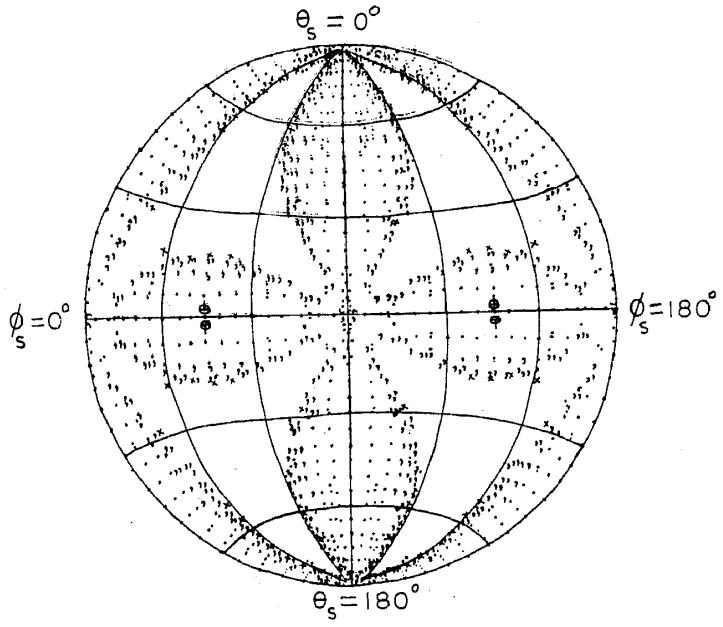

Figure 15. Polar Schmidt-net with Pole at $(\pi/2, \pi/2)$ for the FTA phonons in non-transforming Nb_3Sn at 40 K.

References

Auld B A 1973 *Acoustic fields and waves in solids* (New York: Wiley-Interscience) Vol. 1 p. 368
Eichele R, Huebener R P, Seifert H and Selig K P 1982a *Phys. Lett.* **A87** 469

Eichele R, Huebener R P and Seifert H 1982b *Z. Phys.* **B48** 89
Eisenmenger W 1980 *Phonon scattering in condensed matter* (ed.) H J Maris (New York: Plenum Press) p. 303
Eisenmenger W 1981 *J. Phys. (Paris) Colloq.* **C6** 201
Every A G 1980 *Phys. Rev.* **B22** 1746
Every A G, Koos G L and Wolfe J P 1984 *Phys. Rev.* **B29** 2190
Hensel J C and Dynes R C 1979 *Phys. Rev. Lett.* **43** 1033
Lax M and Narayanamurti V 1980 *Phys. Rev.* **B22** 4876
Mardia K V 1972 *Statistics of directional data* (eds) Z W Birnbaum and E Lukacs (New York: Academic Press) pp. 14–16, 214–218
Maris H J 1971 *J. Acoust. Soc. Am.* **50** 812
McCurdy A K, Maris H J and Elbaum C 1970 *Phys. Rev.* **B2** 4077
McCurdy A K 1982 *Phys. Rev.* **B26** 6971
Northrop G A and Wolfe J P 1979 *Phys. Rev. Lett.* **43** 1424
Northrop G A and Wolfe J P 1980 *Phys. Rev.* **B22** 6196
Philip J and Viswanathan K S 1977 *Pramana* **8** 348
Philip J and Viswanathan K S 1978 *Phys. Rev.* **B17** 4969
Selby B 1964 *Biometrika* **51** 381
Steers J A 1970 *An introduction to the study of map projections* 15th edn (London: University of London Press Ltd.) pp. 78, 79, 222
Taylor B, Maris H J and Elbaum C 1969 *Phys. Rev. Lett.* **23** 416
Taylor B, Maris H J and Elbaum C 1971 *Phys. Rev.* **B3** 1462
Testardi L R 1973 *Physical acoustics principles and methods* (eds) W P Mason and R N Thurston (New York: Academic Press) Vol. X pp. 224, 225, 232, 233
Wolfe J P, Greenstein M, Northrop G A and Tamor M 1980 *Phonon scattering in condensed matter* (ed.) H J Maris (New York: Plenum Press) p. 377